Log-Linear Model for Predicting the Lithium-ion Battery Age based on Resistance Extraction from Dynamic Aging Profiles

Vilsen, Søren Byg; Kær, Søren Knudsen; Stroe, Daniel-Ioan

Published in:
I E E E Transactions on Industry Applications

DOI (link to publication from Publisher):
10.1109/TIA.2020.3020529

Publication date:
2020

Document Version
Accepted author manuscript, peer reviewed version

Log-Linear Model for Predicting the Lithium-ion Battery Age based on Resistance Extraction from Dynamic Aging Profiles

Søren B. Vilsen, *Member, IEEE,* Søren Knudsen Kaer *Member, IEEE,* and Daniel-Ioan Stroe, *Member, IEEE*

***Abstract*—In this work we propose a method for extracting, modelling, and predicting the resistance of Lithium-ion batteries directly from the battery dynamic mission profile. While the extraction of the mainly relied on data manipulation and bookkeeping, the modelling and subsequent prediction of the resistance used a log-linear model. It is shown that the estimated log-linear model can be used to create a posterior probability distribution of the age of the battery, given an internal resistance measurement and the SOC value at which it was measured. This distribution was used calculate the expected age of the battery, and the expected age was compared to weekly check-ups. At an SOC of 80% a mean absolute error (MAE), between the weekly check-ups and the expected age,of 5.83 weeks (706 FEC) was achieved. Furthermore, it is shown that by introducing a decision threshold the MAE could be reduced as far as 2.65 weeks (321 FEC). Lastly, a method is introduced for handling cases where the SOC was not known exactly.**

***Index Terms*—Lithium-ion battery, Resistance estimation, Battery Degradation, Dynamic aging profile, Log-linear model**

I. Introduction

The internal resistance, together with the capacity, is one of the parameters, which describes the performance and lifetime behavior of Lithium-ion (Li-ion) batteries [1]. The internal resistance is used to determine the power capability of batteries [2], which is an important parameter in both renewable energy storage applications and electric vehicle (EV) applications. Thus, by having accurate knowledge about the internal resistance, and subsequently, on the power capability, battery systems can be optimally sized in order to meet both the technical and economic requirements of a certain application. Furthermore, the internal resistance is an important parameter for battery electrical and thermal modeling, as it describes the dynamic and heat generation behavior of the battery, respectively [3], [4].

The internal resistance of Li-ion batteries is a very nonlinear parameter, which is changing depending on the operating temperature, load current, and on the battery state-of-charge (SOC) [3], [5]. Moreover, the internal resistance of the battery is age-dependent, increasing in time during long-term operation [6], [7]. Different methods for determining the internal resistance of the Li-ion batteries exist [8]. However, most of the time, the internal resistance is determined using the current pulse technique, where a charging/discharging current of a certain amplitude and length is applied to the battery and the voltage response of the battery is registered [2], [6]. Then, the internal resistance is calculated using Ohm's Law. This method is successfully applied in laboratory conditions, in order to determine the internal resistance of the battery at different conditions and to track the changes of the internal resistance during battery aging [6]. Nevertheless, a major drawback of this method is represented by the fact that before the resistance measurement, the battery has to be in idling mode, for a certain amount of time (i.e., at least 15 minutes), in order to reach thermo-dynamic stability. Consequently, this requirement makes the method less suitable for real-life applications, where downtime periods of the Li-ion battery storage system is not technical and economic feasible.

As mentioned, if it is possible to perform reference measurements during the aging of the battery, then the effects of aging on the internal resistance can be easily estimated using e.g. a power law function as illustrated in [9], [10]. However, identification of the internal resistance and estimation of the subsequent degradation from a dynamic real-life aging profile requires more sophisticated methods. These methods are usually broken into two categories: online and offline. The most common type of online estimation method is by dual estimation of an equivalent electrical circuit (EEC) based state-space model, and capacity and resistance using a non-linear Kalman-filter variant (i.e. either an extended, or unscented Kalman-filter) [11]–[13], or in some instances the more general particle filters [14], [15]. While yielding seemingly excellent results in some cases, this dual filtering approach introduces too much flexibility into the system. Therefore, the Kalman-filter governing the change in capacity and resistance, is often substituted for a recursive least squares fit with a lag larger than one, adding a higher dependence on previous observations, thereby, providing added stability to the system [16]. This approach can be further improved by basing the state-space model on an Electrochemical model (EM), however, this comes with added computational complexity [17], [18]. Not all online methods are EEC or EM methods a notable exception is the series resistance determination (SRD) algorithm (also called the direct resistance estimation) [16], [19], [20]. The SRD identifies large jumps in current and voltage and uses Ohm's law to calculate a resistance value at the jump. This newly calculated resistance is then used to update the Ohmic resistance by using an exponential moving average. If this approach is to be used for real-life profiles, then it would need to account for different temperatures, the SOC, or the current, which are factors known to influence the resistance. Offline methods are plentiful; they including, but are not limited to, support vector machines (SVM), relevance

vector machines (RVM), genetic algorithms (GA), particle swarm optimisation (PSO), artificial neural networks (ANN, or DNN if the network architecture contains many hidden layers), and appropriate combination of these methods [21]–[27]. These are often called 'black box' methods, because while they are flexible and accurate, extracting how the results are arrived at, is incomprehensible to the human mind. Therefore, recent developments for the offline methods tries combine the flexibility of ANN's, and the stability and knowledge imbued in the EEC framework [24], [25]. However, while the offline methods produce incredibly accurate results, they all suffer from the same restriction: they need large amounts of data to obtain said accuracy.

In this paper, the feasibility of tracking the degradation of the internal resistance directly from a real-life mission profile, which is used to age the battery over a period of 38 weeks, was analysed. The internal resistance is extracted, in a similar fashion to the idea behind the SRD algorithm [16], [19], by keeping careful track of the beginning and length of current pulses. The logarithm of the extracted resistance was assumed to follow a normal distribution, where the mean was a non-linear function of the battery's SOC. The parameters of the internal resistance model were estimated on a week-by-week basis, allowing for the tracking of the changes to the resistance over time. Using the estimated parameters and making assumptions about the prior probability of the SOC and week values, the exact distribution of the battery's age given a new internal resistance value and the SOC at which this was measured can be calculated using Bayes' rule [28] and the law of total probability [28]. Finally, the results, obtained with the proposed method are compared with results obtained from resistance measurement using the traditional method, which were carried out after each week of battery aging.

II. Experiment

A. Lithium-ion battery under test

In this work a cylindrical Li-ion battery cell with a nominal capacity of 2.5 Ah and a nominal voltage of 3.3 V was used. The cell is based on a graphite anode and a lithium iron phosphate (LFP) cathode and it was designed for high power application being able to be continuously charged and discharged with current up to four times the nominal current.

B. Aging condition and internal resistance measurement

The Li-ion battery was aged using the current profile presented in Fig. 1, which has a length of one week. Furthermore, A particularity of the current profile is represented by the fact that in more than 95% of the occurrences a 4C-rate (i.e., 10 A) current was applied for both charging/discharging. When applied to the tested battery cell, the current profile resulted into the battery SOC profile, presented in Fig. 2, which varies in the interval 10% - 90% SOC. The aging profile presented in Fig. 1, containing 121 full equivalent cycles (FECs), was applied for a period of 38 weeks, considering an aging temperature of 25^{o}C. During all 38 weeks aging the current and voltage of the cell was recorded every second. For more details about the aging profile, the reader is referred to [29].

After each week of aging tests, the resistance of the battery was determined using the current pulse technique; the measurements were carried out at 20%, 50% and 80% SOC, considering a current pulse of 4C-rate (i.e., 10 A), which was applied for a length of 18 seconds. Before the current pulse was applied, the battery was in idling mode for 15 minutes, in order to reach thermo-dynamic stability. The obtained increase of the battery resistance during the 38 weeks of cycling is presented in Fig. 3. As one can observe, for the considered aging period, the resistance has increased only by 8.7%, even though the battery cell's capacity decreased by more than 15% in comparison to the value measured at the beginning of life, as it is presented in Fig. 4.

III. Methodology

Extracting the internal resistance of the battery from a dynamic profile, as the one presented in Fig. 1, requires keeping track of the current, I, and of the voltage right before the beginning of the current pulse, V_s. If the current and voltage at a time t, and V_s, were given in advance, one could

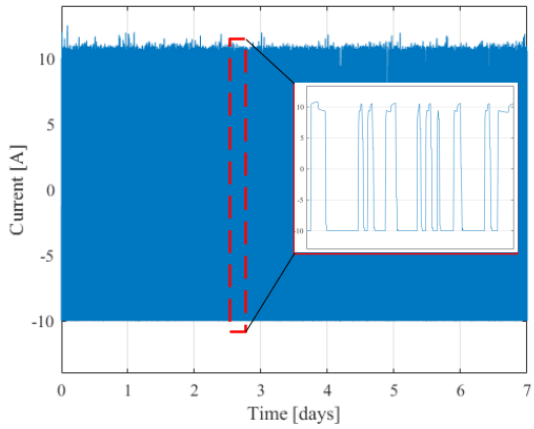

Fig. 1. One-week current profile used for aging the LFP-based Li-ion battery

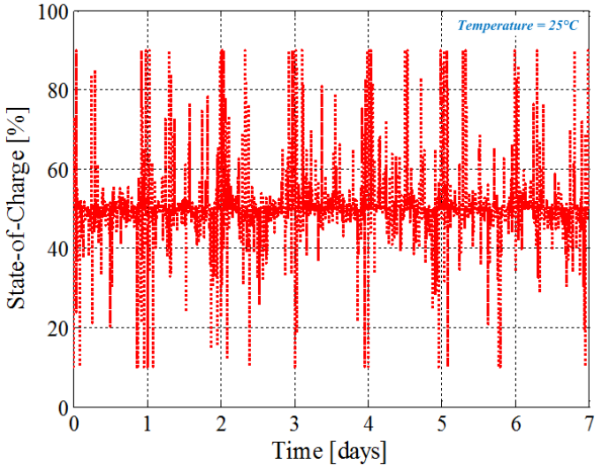

Fig. 2. The battery cell's SOC profile corresponding to one week of aging.

easily calculate the resistance at time t by Ohm's law, Eq. (1), for any given point along a current pulse (i.e. as long as $I_t \neq 0$).

$$R_{i,t} = \left| \frac{V_t - V_s}{I_t} \right| \tag{1}$$

Thus, what remains to be determined is when and how to update V_s. Focusing on the changes of the current from one point in time t, to the next point, $t+1$, the three following situations can be distinguished:

(1) The current changes from zero (i.e., the battery is idling) to a non-zero value (i.e., the battery is either charging or discharging).
(2) The current changes from one non-zero value to another non-zero value.
(3) The current does not change, i.e. the value at time t and $t+1$ are equivalent (within some small difference δ).

In the following, a brief description of the procedure for updating V_s on each of the three aforementioned situations will be given.

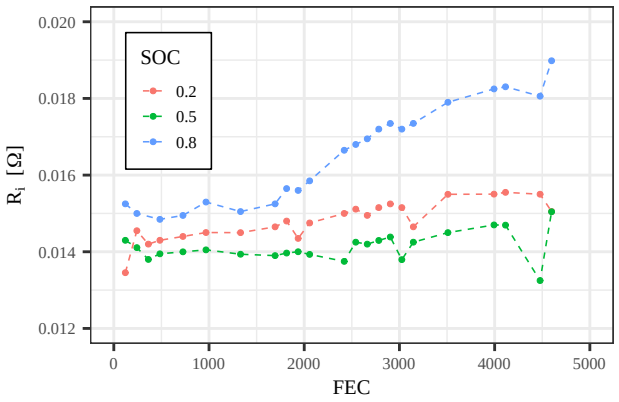

Fig. 3. The internal resistance increase during the aging test.

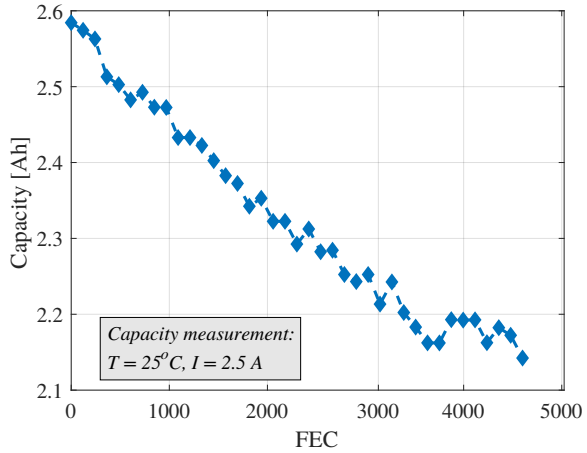

Fig. 4. The capacity fade behavior of the battery cell during the aging test.

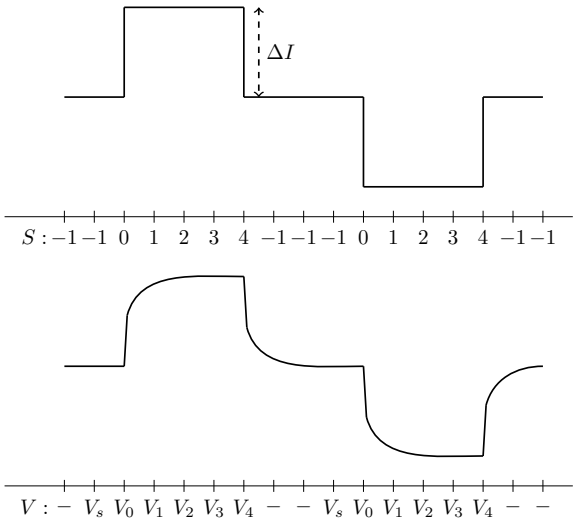

Fig. 5. A simple sketch of the two current pulses with a period of relaxation between pulses (top), and the resulting voltage (bottom).

A. Situation in item (1)

In the first situation, V_s is updated using the voltage of the last instance when the current was zero (i.e. if $|I_t| < \varepsilon$, and $|I_{t+1}| > \varepsilon$), thus, V_s will be equal to V_t. This approach is dependent on the relaxation time between the current pulses, for the battery voltage to reach (or at least get close to) the open circuit voltage (OCV) , i.e. ideally the current profile is shaped as in Fig. 5. The longer the relaxation time between pulses, the more accurate the estimation of the battery resistance.

B. Situation in item (2)

The second case is more complex, but a potential solution will be outlined in the followings. If the time since the battery was idling (i.e. there was no current flowing through the battery) is relatively short (should be optimised), then the currently stored V_s value should be accurate enough for determining the battery resistance. However, the longer the time since the last idling period, the more inaccurate this value is going to be, as sketch in Fig. 6. However, in order to get a model which is as accurate as possible, resistances extracted in this case will be ignored in the remainder of this paper. That is, only the cases where V_s was updated when no current was flowing through the battery were considered. With that said, two possible solutions to this problem could be:

(1) Instead of considering the change in the current from zero, we could consider the change in current from its present value. Consequently, the second situation reverts to the first situation, as seen in Fig. 5. That is, if $|I_t - I_{t-1}| < \varepsilon$, and $|I_{t+1} - I_t| > \varepsilon$, then we set $V_s = V_t$.
(2) If the battery SOC is known and a model of the relationship between the OCV and SOC is available, then the accuracy of the internal resistance estimation can easily be increased using this relationship to update V_s.

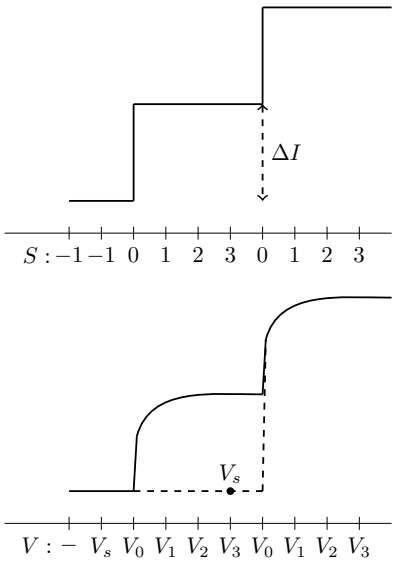

Fig. 6. A simple sketch of the current jumping from one C-rate of ΔI to $2\Delta I$ amperes, with no relaxation between the two C-rates (top), and the resulting voltage (bottom).

C. Situation in item (3)

In the third case, if the current does not change from time t to $t+1$, i.e. $|I_t - I_{t+1}| \leq \delta$, then V_s does not have to be updated. Therefore, we calculate the resistance at time $t+1$ using (1), and move on to the next iteration.

D. Relaxation period

The internal resistance is largely dependent on the length of the current pulse, as it is presented in [5]. Furthermore, after the current has been interrupted, it takes time for the battery to reach thermo-dynamic stability. Therefore, it is useful to also track the length of the previous pulse, L, and the length of any previous relaxation period T. Thus, it may be beneficial to restrict ourselves to resistances, which had longer relaxation times before updating V_s such that the voltage has time to stabilise. The effect of the relaxation period on the performance of the extraction method was investigated by comparing the results of: (1) resistance identification requiring that the relaxation period has to be at least as long as the previous current pulse (i.e. where $T \geq L$), and (2) resistance identification requiring only one second of relaxation (i.e. where $T \geq 1$). The internal resistance extracted in the two cases will be denoted as R_i and $\tilde{R}_i$, respectively.

E. The characteristics of the estimated internal resistance

As the internal resistance was measured after each week of aging using a pulse length of 18 seconds, then the internal resistance extracted using the proposed methodology was defined as the resistance value after 18 seconds, i.e. $R_i = R_{i,18s}$. Furthermore, the considered dynamic aging profile, presented in Fig. 1, is characterized by many changes of the current all of the same C-rate amplitude. Thus, the internal resistance of the battery was estimated only for current values in the interval 9.5 A – 10.5 A, which allowed for (1) isolating the dependence of the internal resistance on the current, and (2) an unbiased validation of the proposed method.

IV. Results

A. Internal resistance variation with SOC

By isolating the effects of the temperature, current (i.e., C-rate), and pulse length, the internal resistance of the tested battery cell, varies only with the SOC and increases while the battery is aging.

Based on previous studies [3], [5], it is well known that the internal resistance of the battery increases when approaching very low and very high SOCs. Thus, the dependence of the internal resistance on the SOC was expressed using:

$$R_i(\text{SOC}) = a \cdot \text{SOC}^b (1 - \text{SOC})^c, \tag{2}$$

where SOC takes values between 0 (fully discharged battery) and 1 (fully charged battery), and $a > 0$, while $b, c \leq 0$. Furthermore, considering the logarithm of (2), the relationship becomes linear in the parameter space, which is highly desirable for parameter estimation. Therefore, it is assumed that the logarithm of the battery resistance for a given aging week w, is:

$$\begin{aligned} \log(R_i) = \beta_{0,w} + \beta_{1,w} \cdot \log(\text{SOC}) \\ + \beta_{2,w} \cdot \log(1 - \text{SOC}) + \varepsilon, \end{aligned} \tag{3}$$

where ε follows a normal distribution with mean zero variance σ^2. Furthermore, it is assumed that the variance does not change from week-to-week. The parameters in (3) are estimated by maximum likelihood [28] under the assumption that $\beta_{1,w}$ and $\beta_{2,w}$ are both smaller than, or equal to, 0.

The internal resistance model, described by Eq. (3), does not account for the direction of the current, i.e. charging or discharging the model does not change. This is not necessarily desirable if there is a large difference in the internal resistance between charging and discharging. The model can be extended to account for the current direction, by forcing the three parameters, describing the expected internal resistance (i.e. $\boldsymbol{\beta}$), to be direction dependent. This comes at the cost of more parameters (a total of 7 parameters instead of the 4 needed in the model not accounting for direction), and it requires that the internal resistance can be extracted across a SOC domain for both charging and discharging. Preliminary analysis showed that the difference in the extracted internal resistance between charging and discharging was minimal given the estimated variation of the model. Therefore, in the remainder of the paper, when referring to the resistance model will imply the model described in Eq. (3).

The internal resistance values extracted based on the considered aging profile and using the methodology presented in the previous section are illustrated in Fig. 7 and Fig. 8, for three different degradation levels of the battery cell. The results presented in Fig. 7 were obtained requiring a relaxation period T equal to the length of the previous current pulse, while the results presented in Fig. 8 were obtained requiring a relaxation period T equal to one second.

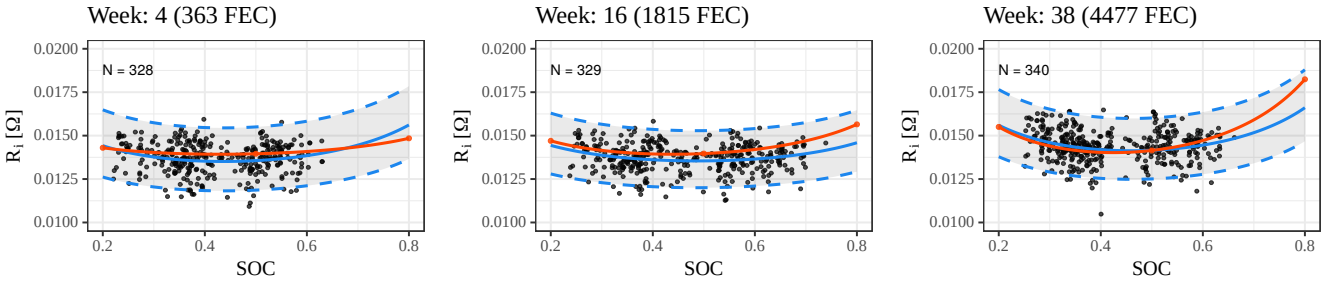

Fig. 7. The internal resistance obtained during the periodic check-ups (traditional approach) and the internal resistance extracted from the dynamic profiles (investigated approach) against the SOC, shown as red points (•) and black points (•), respectively. The extracted internal resistance was obtained considering a relaxation period at least as long as the previous current pulse (unlike Fig. 8 where only 1 second of relaxation is required). While the relationship between the internal resistance and the SOC was depicted at three levels of ageing: 4 weeks (left), 16 weeks (center), 38 weeks (right). The internal resistance model was fitted to the red and black points, illustrated by the red line (——) and blue line (——), respectively. The shaded area bounded by the dashed blue lines (- - -) is a 95% confidence interval of the expected internal resistance (for the model fitted to the extracted internal resistance).

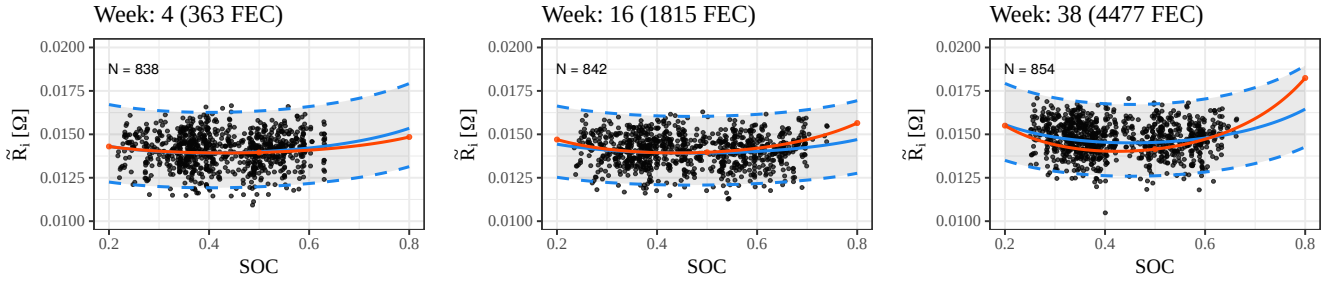

Fig. 8. The internal resistance obtained during the periodic check-ups (traditional approach) and the internal resistance extracted from the dynamic profiles (investigated approach) against the SOC, shown as red points (•) and black points (•), respectively. The extracted internal resistance was obtained considering a relaxation period of 1 second from the previous current pulse (unlike Fig. 7 where a relaxation period at least as long as the previous pulse is required). While the relationship between the internal resistance and the SOC was depicted at three levels of ageing: 4 weeks (left), 16 weeks (center), 38 weeks (right). The internal resistance model was fitted to the red and black points, illustrated by the red line (——) and blue line (——), respectively. The shaded area bounded by the dashed blue lines (- - -) is a 95% confidence interval of the expected internal resistance (for the model fitted to the extracted internal resistance).

The internal resistance values estimated using the proposed methodology (black dots in Fig. 7 and Fig. 8) have been fitted using the model (2), where the blue line is the exponential of the expected log-resistance and the shaded area represents the 95% confidence interval. Furthermore, the red dots and the red dashed lines represent the internal resistance values extracted from the weekly check-ups and the model fitted to the extracted resistances at that corresponding week, respectively.

B. Comparing relaxation times

Comparing the results obtained for the two considered relaxation periods, it can be observed that while the number of internal resistance values is reduced by more than half, when imposing a stricter relaxation period requirement, the variation is also drastically reduced. This is clearly seen in Fig. 9, which shows histograms of the standard deviation of the models fitted to the resistance extracted with the stricter relaxation requirement on the left, and only one second of relaxation shown on the right.

In order to verify the accuracy of the proposed methodology for extracting the battery internal resistance from a dynamic mission profile, two approaches are considered:

(1) The absolute percentage error (APE) between the expected internal resistance of the weekly check-ups at the end aging period, μ^*, and internal resistance extracted from the dynamic profile using the proposed methodologies, y:

$$\text{APE} = \left| \frac{\mu^* - y}{\mu^*} \right|, \tag{4}$$

The expected internal resistance, μ^*, is the red curve seen in Fig. 7 and 8. While y represents $\log(R_i)$ or $\log(\tilde{R}_i)$ and is seen as the black points in Fig. 7 or 8, respectively.

(2) The integrated squared error (ISE) between the expected internal resistance of the weekly check-ups at the end aging period, μ^*, and the expected internal resistance extracted from the dynamic profile using the proposed methodologies, $\hat{\mu}$:

$$||\mu^* - \hat{\mu}||_2 = \left(\int_0^1 \left(\mu^*(S) - \hat{\mu}(S)\right)^2 dS \right)^{(1/2)} \tag{5}$$

The expected internal resistances, $\hat{\mu}$, correspond to the blue lines in Fig. 7 and 8, dependent on if the relaxation time was restricted to being at least as long as the previous pulse, or a single second, respectively.

The values of the median APE for the 38 weeks are shown for both considered relaxation periods in Fig. 10. By comparing the obtained median APE's for the two relaxation periods, one can observe that the added restriction on the

relaxation period, yields smaller median APE, as expected due to the smaller variance (see Fig. 9). Furthermore, it has to be highlighted that the median APE presented on the left panel of Fig. 10 is smaller than 4.5% in all but three cases. These results strongly suggest that the proposed internal resistance identification method can be used as an alternative approach for the traditional method, which needs the battery to be on stand-by for at least 15 minutes before the resistance measurement.

The ISE's for all 38 weeks and both relaxation methods are summarised as a histogram in Fig. 11. The figure shows that the ISE between the expected resistance during the weekly check-ups and the expected extracted resistance were almost identical irrespective of the two relaxation requirements. That is, if the only thing of interest is the expected behaviour of the resistance (i.e. the mean function), then using either relaxation method will yield almost equivalent results. However, this model is going to be used to predict battery age; therefore, it will be beneficial to keep the variance as small as possible, as it will make it easier to distinguishing the resistance at different stages of aging, and at different SOCs. Thus, from this point forward, when referring to the extracted resistance, or parameters of the corresponding log-linear model, it will always be in reference to the resistance extracted using a relaxation time at least as long as the previous pulse.

C. Estimated parameters over time

Fig. 12 shows the change in the estimated parameters of the log-linear resistance model over time. The figure shows that over time the $\boldsymbol{\beta}$ parameters decrease, while the standard deviation of the model decreases in the beginning, but steadily increase from around week 9 (1089 FEC). The decrease in $\beta_{1,w}$ and $\beta_{2,w}$ results in an increased (expected) internal resistance towards the edges of the SOC domain (i.e. close to 0 or 1). The smaller the parameter, the faster, and more drastic, the increase in the internal resistance. Thus, the figure shows that the resistance increases faster as the SOC tends towards 1 (as $\beta_{2,w}$ is smaller than $\beta_{1,w}$) compared to the SOC tending towards 0. The $\boldsymbol{\beta}$ parameters together are used to control the minimum expected internal resistance (at a SOC of 0.5). This, as seen in Fig. 7, stayed fairly consistent across time. Thus, if $\beta_{1,w}$ and $\beta_{2,w}$ decrease over time resulting in an increased internal resistance, then $\beta_{0,w}$ has to decrease to keep the minimum expected internal resistance consistent.

D. Prediction of the battery age

Based on the model described in the previous section, the battery internal resistance can be accurately predicted, given a SOC value and the battery age (i.e., the week value). However, estimating the battery's age (i.e., week) knowing the resistance value and the SOC at which it was determined is also of interest; to be more precise, the probability distribution of $\mathbb{P}(w|R_i, \text{SOC})$ has to be determined. In order to evaluate this distribution, something has to be assumed about the probability distribution of the SOC, the week, and the joint distribution of resistance, SOC, and week. Starting with the joint distribution, by the definition of conditional probabilities [28] and under the assumption that the SOC and week are independent (which must be true), it can be written:

$$\begin{aligned}\mathbb{P}(\log(R_i), \text{SOC}, W) = \\ \mathbb{P}(\log(R_i)|\text{SOC}, W)\mathbb{P}(\text{SOC})\mathbb{P}(W).\end{aligned} \tag{6}$$

Thus, the joint distribution can be split into three parts, $\mathbb{P}(\log(R_i)|\text{SOC}, W)$, $\mathbb{P}(\text{SOC})$, and $\mathbb{P}(W)$. The conditional distribution of the internal resistance given the SOC and week, $\mathbb{P}(\log(R_i)|\text{SOC}, W)$, is the model described in the previous section. Furthermore, the marginal distributions of the SOC and week, $\mathbb{P}(\text{SOC})$ and $\mathbb{P}(W)$, respectively, have to be defined. In this context, these distributions should be interpreted as a priori information. That is, if any prior information about the distribution of SOC or week are known, they should be considered at this point. However, in this paper, it will be assumed that any value of SOC and week is equally likely a priori. Consequently, it is assumed that the battery SOC follows a continuous uniform distribution on the unit interval and the week will follow a discrete uniform distribution over the set of possible weeks. Following this reasoning, the posterior distribution of the weeks, given the battery resistance and SOC can be calculated using:

$$\begin{aligned}\mathbb{P}(W|\log(R_i), \text{SOC}) = \\ \frac{\mathbb{P}(\log(R_i)|\text{SOC}, W)\mathbb{P}(\text{SOC})\mathbb{P}(W)}{\sum_{w=1}^{\#\text{no. total weeks}} \mathbb{P}(\log(R_i)|\text{SOC}, w)\mathbb{P}(\text{SOC})\mathbb{P}(w)}\end{aligned} \tag{7}$$

The posterior distribution (7) follows from the application of Bayes rule and the law of total probability to (6). The exact distribution of the battery cell week will be summarised by its weighted median and high posterior density region (HPD). A 95% HPD region represents the smallest possible combination of regions with a combined probability (area beneath the curve) of 95%.

Fig. 13 shows the exact posterior probability of the week, given an internal resistance of 15 mΩ measured at SOC's of 20, 50, and 80%, respectively. These figures, in general, show a very consistent posterior probability across weeks, at around 2-4%. In particular, given a resistance of 15 mΩ, the posterior distributions at 20 and 80% SOC are almost identical, although we see that it is slightly more likely that the battery was 35 weeks (or older) if the resistance was measured at 20% SOC, than at 80% SOC. These sound like small probabilities, but looking at Fig. 7, we see that by drawing a line at 0.015 Ω on the ordinate axis, it would be almost exactly in the middle of all three confidence intervals. This can also be observed by the weighted median which ranged 17.4 – 24.7 weeks, and the 95% HPD regions, the blue shaded area of the figures, which stretches over the entire considered aging period (i.e., weeks 1 to 38) in all three figures – making the HPD useless for interpretation in this case. This is to be expected, as the battery's internal resistance only increased by 8.7% during the 38 weeks of aging, as seen in Fig. 3. Furthermore, the difference between the posterior distributions at 20 and 80%

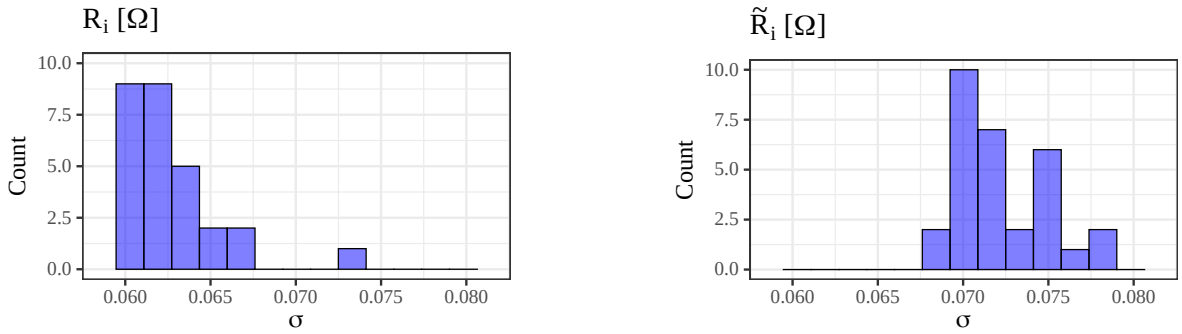

Fig. 9. Histogram of the estimated standard deviation of the log-linear resistance model fitted to every week of the extracted resistance. In the left panel a relaxation period at least as long as the previous current pulse was required, while the resistances extracted for the right panel only required a single second of relaxation.

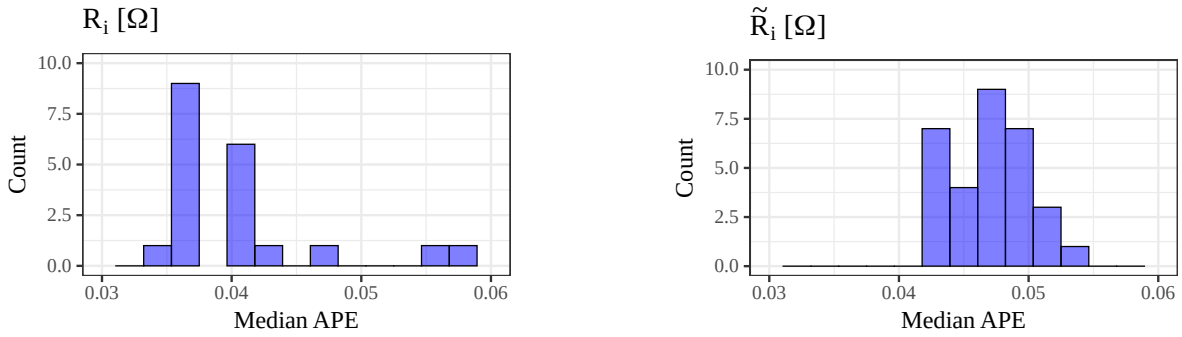

Fig. 10. Histogram of the median APE of every week for the extracted resistance. On the left panel a relaxation period at least as long as the previous current pulse was required, while on the right panel only required a single second of relaxation.

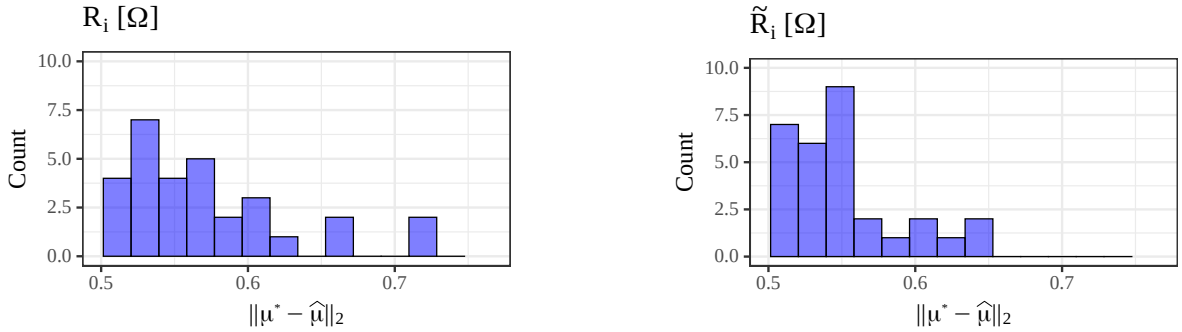

Fig. 11. Histogram of the integrated squared difference of every week, between the expected resistance of the weekly check-ups, and the expected extracted resistance. On the left panel a relaxation period at least as long as the previous current pulse was required, while on the right panel only required a single second of relaxation.

SOC should also be expected because the parameter $\beta_{2,w}$ decreases faster than $\beta_{1,w}$, as seen in Fig. 12.

Fig. 14 shows the exact posterior probability of week, when the internal resistance was increased from 15 mΩ to 20 mΩ, and the SOC was kept at 20, 50, and 80%, respectively. Similar with an internal resistance of 15 mΩ, the posterior probability distributions at 20 and 80% SOC are almost identical. The HPD regions show that the batteries have a 95% probability of being older than 22.8 and 27.5 weeks given that the internal resistance of 20 mΩ was measured at 20% and 80% SOC, respectively. This is also seen from the blue shaded area in the corresponding figures. In both cases, the mode of the distribution (its highest point) is at 38 weeks with a probability larger than 0.2, and the weighted median week is around 35. This is also reflected in the posterior distribution at 50% SOC, with a mode at 38 weeks where the probability is slightly larger than 0.15. However, at 50% SOC we also see a higher probability around weeks 1-10, as seen from the 95% HPD which is the union of $[1; 12]$ and $[23; 38]$. This is caused by an initial decrease in the internal resistance, measured at around 50% SOC, during the first few weeks of aging. Furthermore, this phenomenon is magnified by the fact that the internal resistance does not increase as much at 50% SOC, when compared to 20% and 80% SOC – this is also seen by comparing the trajectories of the curves corresponding to each of the three SOC values, which can be seen in Fig. 3.

Lastly, the periodic check-ups performed at the end of each week will be used to illustrate how these distributions could be

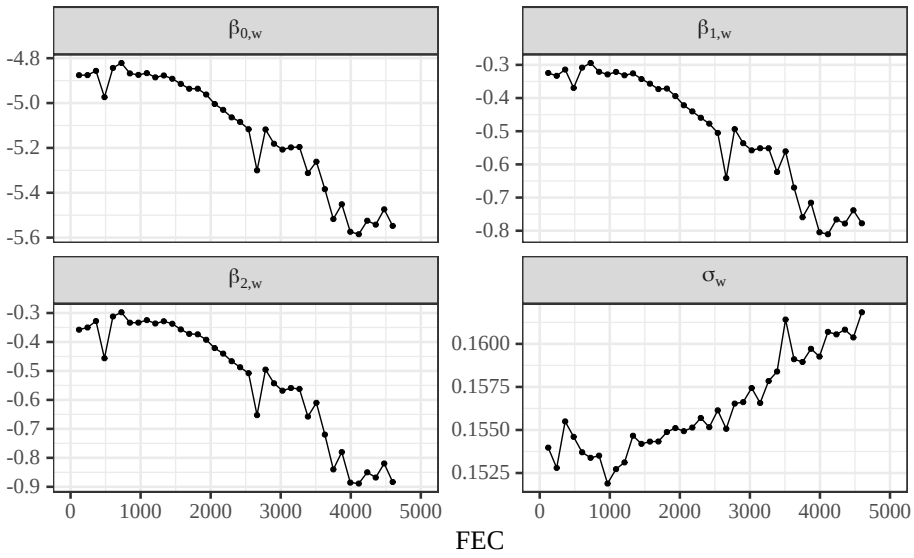

Fig. 12. The parameter estimates of the log-linear resistance model, given resistances extracted using a relaxation time larger to or equal to the length of the previous current pulse, for every week.

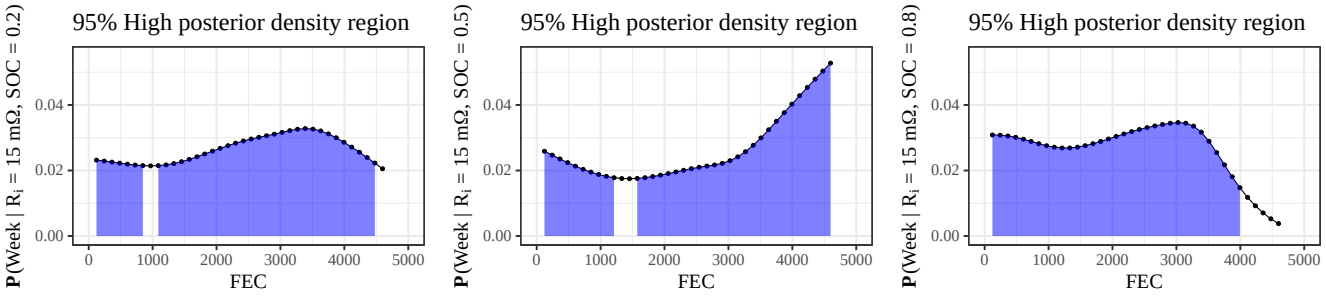

Fig. 13. The posterior distribution of the battery ageing week given an internal resistance of 15 mΩ, and a SOC of 20, 50, and 80%, shown on the left, in the middle, and on the right, respectively.

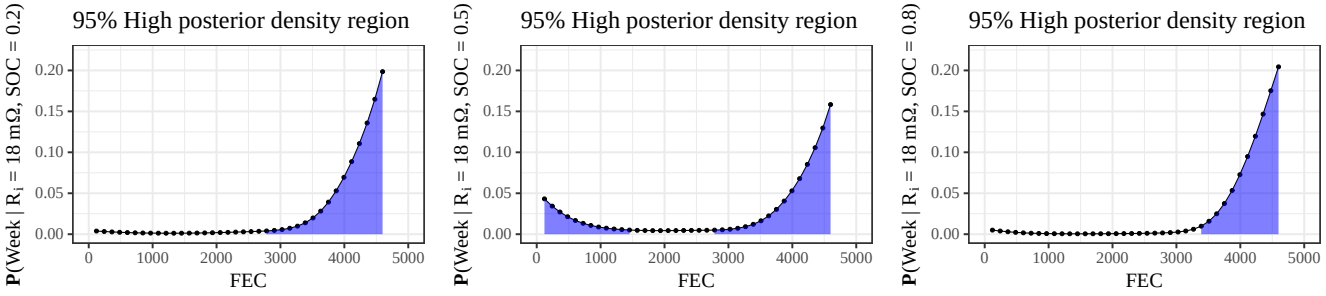

Fig. 14. The posterior distribution of the battery ageing week given an internal resistance of 18 mΩ, and a SOC of 20, 50, and 80%, shown on the left, in the middle, and on the right, respectively.

used to predict the FEC. Two measures will be used to evaluate the performance of the predictions made using probability distribution in Eq. (7):

(1) The percentage of cases where the week of the check-up is within the 95% HDR of the distribution (which should be approximately 95%).
(2) The mean absolute error (MAE) between the expected week of the distribution and the week of the check-up. Where the expected week, $\hat{w}$, of a given probability distribution, is given by:

$$\hat{w} = \sum_{w=1}^{\#\text{no. total weeks}} w \cdot p_w, \tag{8}$$

where p_w is the probability of week w, seen in Eq. (7).

The percentage of cases the week of the periodic check-up was within the 95% HDR of its constructed distribution was 94.6%, and the MAE between the expected and check-up

weeks were 937.75 FEC (7.75 weeks). While the HDR result is adequate, the MAE leaves something to be desired. However, if the MAE is split on a SOC-by-SOC basis, the MAE at 20, 50, and 80% is 976.47, 1122.88, and 705.43 FEC, respectively (corresponding to 8.07, 9.28, and 5.83 weeks). That is, most of the error is created at 20 and 50%. The reason for the large error is due to the flatness of the probability distribution, as seen in Fig. 13 for distributions corresponding to 20 and 80% SOC. If the distribution is horizontal line, the probability (i.e. the height) would have to be $1/38$ (≈ 0.026). This statement can be reversed, i.e. if the largest probability is around 2.6%, the resulting curve would have to be almost entirely flat. A flat curve further implies a $\hat{w}$ value close to the average number of weeks. This leads to a lot of predictions around 1633.5 FEC (13.5 weeks), increasing the prediction error.

However, a threshold could be introduced requiring that the largest probability of the distribution is larger than 5%. If only using cases where the probability is above this threshold, would mean avoiding making predictions in cases where there is no definitive answer, at the cost of making less predictions. Setting the threshold at 5%, the MAE for 20, 50, and 80% SOC are 534.82, 2084.83, and 320.65 FEC, respectively (corresponding to 4.42, 17.23, and 2.65 weeks). However, the number of cases where the largest probability was above the threshold was 4, 2, and 17, for the internal resistance values found at 20, 50, and 80% SOC, respectively.

E. Prediction of the battery age with unknown SOC

Predicting the battery's age using Eq. (7) has one obvious flaw: it requires exact knowledge of the SOC at the time the resistance is measured. Under laboratory conditions, this is not an issue, as simple methods (i.e., Coulomb counting, open circuit voltage measurement), which are considering certain assumptions, can be successfully applied; however, in real-life applications, the proposed SOC estimation methods are still subjected to errors and/or increased computational burden. Thus, it would be desirable to estimate the battery age, without knowing the SOC at which the battery resistance is measured. This becomes possible by considering a small modification to Eq. (7) to account for the added uncertainty on the location of the SOC:

$$\mathbb{P}(W|\log(R_i)) = \frac{\int_0^1 \mathbb{P}(\log(R_i)|S,W)\mathbb{P}(S)\mathbb{P}(W)dS}{\sum_{w=1}^{\#\text{no. total weeks}} \int_0^1 \mathbb{P}(\log(R_i)|S,w)\mathbb{P}(S)\mathbb{P}(w)dS}, \quad (9)$$

i.e. the uncertainty can be accounted for by specifying a distribution of the SOC (representing the uncertainty of the location), and integrating both numerator and denominator over the domain of the SOC. The uncertainty associated with the prior distribution represents the measurement error of the SOC estimate. Furthermore, given an SOC estimate and a desired precision, a prior distribution can easily be constructed. As an example, assume the SOC is estimated to be 0.8, and it is very likely within the interval $[0.75; 0.85]$, two possible choices of prior distribution (out of many) could be:

(1) A uniform distribution on the interval $[0.75; 0.85]$. This will ensure that the SOC can not take values outside the interval (i.e. there is 100% chance the SOC is within the interval). However, it weights every choice of SOC within the interval equally, i.e. the additional information that the SOC is estimated at 0.8 is not used.
(2) A beta distribution with mean 0.8 and variance 0.001. This says that the expected SOC is 0.8, but that there is a 95% probability of the SOC being within $[0.74; 0.85]$. Thus, incorporating the additional information of the expected location of the '*true*' SOC. Note: that using this prior distribution implies that the SOC could technically be anywhere between 0 and 1, but that the probability of it being less than 0.75, and larger than 0.85 is 5%.

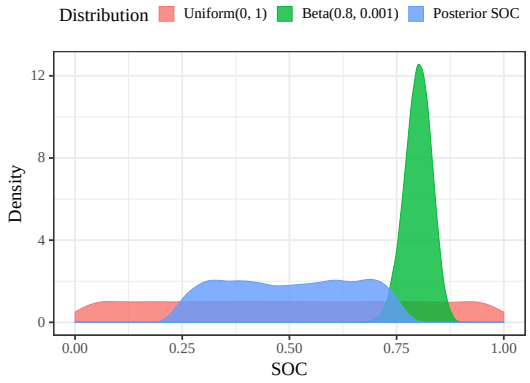

Fig. 15. Density of the a priori knowledge on the location of the SOC.

Fig. 15 shows contains three examples of prior distributions on the SOC, in the form of density functions: (1) a uniform distribution on the entire unit interval, (2) a posterior distribution of the SOC learned from the aging data (in a similar manner to Eq. (7) and (9)), and (3) a beta distribution with a mean of 0.8 and a variance of 0.001. The uniform, posterior, and beta distributions are shown in red, blue, and green, respectively. The interpretation of the uniform distribution is simply that the SOC is entirely unknown, i.e. it could be anywhere between 0 and 1. The posterior SOC distribution is not much better, but it takes into account the previous usage of the battery cell. That is, from the density in Fig. 15, the battery is operated on the interval $[0.2; 0.8]$, and the majority of that time is spend in $[0.25; 0.75]$. Both intervals are very large, and will increase the uncertainty of any prediction made using these prior distributions. The beta distribution, as mentioned above, states that the SOC is most likely 0.8, and is a 95% certainty within 0.74 and 0.85. Note that both the uniform distribution on the entire unit interval and the learned posterior SOC distributions are only really useful if nothing is known about the SOC.

The effect of the added variability (added by not knowing the '*true*' location of SOC) on the posterior distribution of the battery's age, are shown in Fig. 16 for the three SOC distributions shown in Fig. 15, given internal resistances of

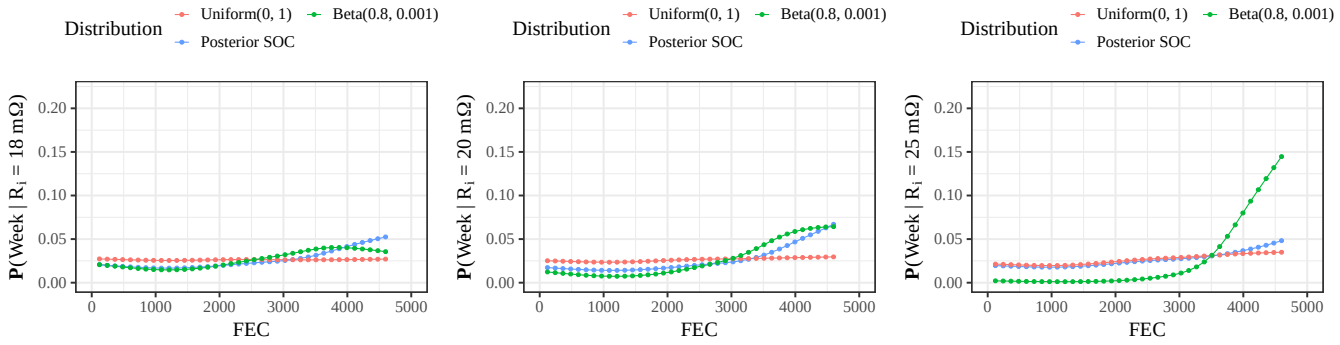

Fig. 16. The posterior distribution of the battery aging week given an internal resistance and a distribution over the SOC. The distributions uniform on $[0; 1]$, beta with mean 0.8 and variance 0.01, and the posterior SOC (learned from the aging data), shown in red, green, and blue, respectively. Furthermore, the posterior distributions are shown for a measured resistance of 18, 20, and 25 mΩ, shown from left to right.

18, 20, and 25 mΩ, are shown in Fig. 16 for the three SOC distributions shown in Fig. 15. As it was illustrated in Fig. 13 and 14, the point at which the SOC is measured has a large influence on the posterior probability distribution. Fig. 16 shows that if the location of the SOC is entirely unknown (i.e. the SOC distribution is entirely uniform) the posterior distribution is almost a flat line, i.e. the battery could be any age, even for very large resistance values. The SOC distribution learned from the data, shows slightly better results are achieved (when the left most panel of Fig. 16 is compared to the three panels of Fig. 14), if the guess of the SOC's location is limited to the way the battery has been used until this point. Lastly, the green line showing the posterior distribution, when assuming the SOC is located around 80% (using a beta distribution), should resemble the right-most panel of Fig. 14, when the variance is small. However, the left-most panel clearly shows that having a variance of 0.001 (resulting in a 95% credibility interval of $[0.74; 0.85]$), is to much to confidently determine the probability of the battery's age at a resistance of 18 mΩ. It requires a much larger resistance value to get a high mode of the posterior probability of the battery age.

The SOC priors were chosen to illustrate the general concept of the method; in reality most SOC estimation methods are within $\pm 1\%$ [30]. As a result in order to show any real change in the probability distributions, the internal resistance values had to be fairly large. Thus, the values 18, 20, and 25 mΩ are not directly related to the analysed battery cell. With that said, they are well within the realm of possible values for further degradation of the battery.

F. Generalization of the proposed model

If the model should be used in an application with variable temperature and C-rate, the model needs to be extended to account for changes in to these variables. The simplest possible case assumes that both temperature and C-rate do not interact with SOC, or each other, and their relationship with the resistance is additive on a log-scale (multiplicative on a linear-scale).

If the relationship between temperature and the resistance is similar to a Arrehnius relationship, then the model accounting for SOC and temperature could look as follows:

$$\begin{aligned}\log(R_i(\text{SOC}, T)) = \tilde{\beta}_0 &+ \beta_1 \log(\text{SOC}) \\ &+ \beta_2 \log(1 - \text{SOC}) \\ &+ \beta_3 \frac{1}{T} + \tilde{\varepsilon}.\end{aligned} \tag{10}$$

The $\tilde{\beta}_0$ no longer has the same interpretation as for the model presented in the paper (hence the added tilde), as it now contains both the β_0 from the model in the paper, and the pre-exponential factor of a Arrhenius equation. With that said, the parameter β_3 could be interpreted as the ratio of the activation energy and the universal gas constant (or equivalently the Boltzmann constant). Furthermore, the noise component $\tilde{\varepsilon}$, would also differ from the one presented in the paper, as the variance induced by this component would be different.

If the relationship between the resistance and C-rate is assumed to follow an exponential decay function with equal decay rate for both charging and discharging, then the model in Eq. (10) can be extended to:

$$\begin{aligned}\log(R_i(\text{SOC}, T, I)) = \tilde{\tilde{\beta}}_0 &+ \beta_1 \log(\text{SOC}) \\ &+ \beta_2 \log(1 - \text{SOC}) \\ &+ \beta_3 \frac{1}{T} + \beta_4 |I| + \tilde{\tilde{\varepsilon}}.\end{aligned} \tag{11}$$

As above $\tilde{\tilde{\beta}}_0$ does not have the same interpretation contains the β_0 from the model in the paper, the pre-exponential factor of a Arrhenius equation, and an scaling factor from the exponential decay. The same is true for the noise component $\tilde{\tilde{\varepsilon}}$. The current, I, in the equation above could be substituted for C-rate (i.e. I/Q_{norm}, where Q_{norm} is the nominal capacity) to introduce some stability and generalisability to the model. Furthermore, the current direction can also be accounted for in a similar fashion as described in Section IV(A). The model shown in Eq. (11) only represents a first order relationship between the current (or C-rate) and the internal resistance, however, extension to the model accounting for higher order relationships should be possible.

If the relationship between the internal resistance and the

variables SOC, temperature, and current cannot be assumed to be additive on a log-scale, then parameter estimation gets a lot more complicated (even if the relationship is additive on the linear-scale – a relatively simple alternative).

However, without the necessary data, accepting, or rejecting, the model in Eq. (11) is impossible. As would be the derivation of a more complicated model. Therefore, these extensions are only presented, and not validated in this paper.

V. Conclusions

In this paper, a methodology was proposed for identifying the battery internal resistance and model its degradation behavior directly from a dynamic aging profile. The resistance was extracted by keeping careful track of the changes to the current profile and, then, calculating the resistance of any given point in time, using Ohm's law. The internal resistance was defined as the resistance extracted after 18 seconds of consistent charging, and further limited to resistances calculated following a period of relaxation at least as long as the previous current pulse.

The extracted internal resistance for a given week, was then modelled as a log-linear function of SOC. The model fitted to the extracted internal resistance was extremely consistent with the internal resistance obtained by a traditional method, and could easily be incorporated into a framework for finding the posterior probability distribution of battery cell being w weeks old, given an internal resistance measured at a SOC value. The analysis showed that the extracted internal resistance was fairly stable across weeks in, and around, 50% SOC, when compared to 20 and 80% SOC, where the internal resistance increased at a much higher rate. This was in complete concordance with the internal resistance obtained by traditional methods. The constructed probability distributions were used to predict the expected age of the battery, given SOC and internal resistance, and the performance was quantified by using the weekly check-ups. The resulting MAE for 20 and 50% SOC were both above 968 FEC (8 weeks), while the MAE at 80% SOC was slightly smaller than 726 FEC (6 weeks). However, if a threshold was introduced, then the MAE at 80% SOC was reduced to (2.65 weeks), but it reduced the number of useful measurements from 32 to 17. The introduction of a threshold is not ideal. In an ideal world the variance of the extraction process should be reduced, in order to achieve better performance.

The presented framework was then extended to cases where the SOC was not known precisely, but a probability distribution over its possible location of the SOC could be specified. It was shown that this distribution needed to have a narrow 95% credibility interval to achieve results comparable to when an exact SOC value was available. Lastly, this framework lends itself readily for an extension to estimating the battery's remaining useful life (RUL), as the posterior probability distribution of the week values can be directly translated to the RUL of the battery. However, this is left for future research.

Acknowledgements

This work has been part of the "CloudBMS – The New Generation of Intelligent Battery Management Systems" research and development project, project number 64017-05167. The authors gratefully acknowledge EUDP Denmark for providing the financial support necessary for carrying out this work.

Furthermore, the authors like to thank Poul Svante Eriksen for his help developing some of the ideas in the early stages.

Lastly, the authors would like to thank the two reviewers for their insightful comments, which improved the paper.

References

[1] T. Reddy, "Linden's Handbook of Batteries," 4th edition, McGraw Hill, 2010.

[2] Electrically propelled road vehicles – Test specification for lithium-ion traction battery packs and systems – Part 1: High-power applications, ISO 12405-1:2011.

[3] A.-I. Stroe, "Analysis of Performance and Degradation for Lithium Titanate Oxide Batteries," PhD Thesis, Aalborg University, 2018.

[4] N. Nieto et al., "Thermal Modeling of Large Format Lithium-Ion Cells," Journal of The Electrochemical Society, vol. 160, pp. A212-A217, 2013.

[5] B.V. Ratnakumar, M.C. Smart, L. D., Whitcanack, R. C. Ewell, "The impedance characteristics of Mars Exploration Rover Li-ion batteries," Journal of Power Sources, vol. 159, pp. 1428-1439, 2006.

[6] D.-I. Stroe, M. Swierczynski, S.K. Kær, R. Teodorescu, "Degradation Behavior of Lithium-Ion batteries during Calendar Ageing – The Case of the Internal Resistance Increase," IEEE Transactions on Industry Applications, vol. 54, pp. 517-525, 2018.

[7] M. Ecker, N. Nieto, S. Kabitz, J. Schmalstieg, H. Blanke, A. Warnecke, D. U. Sauer, "Calendar and cycle life study of Li(NiMnCo)O2-based 18650 lithium-ion batteries," Journal of Power Sources, vol. 248, pp. 839-851, 2014.

[8] H.-G. Schweiger et al., "Comparison of Several Methods for Determining the Internal Resistance of Lithium Ion Cells," Sensors, vol. 10, pp. 5604-5625, 2010.

[9] D.-I. Stroe, M. Swierczynski, S.K. Kær, E. Martinez-Laserna, and E. Sarasketa-Zabala, "Accelerated Aging of Lithium-Ion Batteries based on Electric Vehicle Mission Profile," 2017 IEEE Energy Conversion Congress and Exposition (ECCE), Cincinnati, OH, pp. 5631-5637, 2017.

[10] T.R.B. Grandjean, J. Groenewald, A. McGordon, W.D. Widanage, J. Marco, "Accelerated Internal Resistance Measurements of Lithium-Ion Cells to Support Future End-of-Life Strategies for Electric Vehicles, " Batteries, vol. 49, 2018.

[11] Y. Liu, Z. He, M. Gao, Y. Li, G. Liu, "Dual Estimation of Lithium-ion Battery Internal Resistance and SOC Based on the UKF," 2012 5th International Congress on Image and Signal Processing, Chongqing, pp. 1639-1643, 2012.

[12] Y. Fang, R. Xiong, J. Wang, "Estimation of Lithium-Ion Battery State of Charge for Electric Vehicles Based on Dual Extended Kalman Filter," Energy Procedia vol. 152, pp. 574-579, 2018

[13] Y. Zou, X. Hu, H. Ma, and S.E. Li, "Combined State of Charge and State of Health estimation over lithium-ion battery cell cycle lifespan for electric vehicles," Power Sources, vol. 273, pp. 793-803, 2015.

[14] H. He, R. Xiong, H. Guo, and S. Li, "Comparison study on the battery models used for the energy management of batteries in electric vehicles," Energy Convers. Manag. vol. 64, pp. 113–121, 2012.

[15] S. Schwunk, N. Armbruster, S. Straub, J. Kehl, and M. Vetter, "Particle filter for state of charge and state of health estimation for lithiume-iron phosphate batteries," Power Sources, vol. 239, pp. 705-710, 2013.

[16] M. Mathew, S. Janhunen, M. Rashid, F. Long, and M. Fowler, "Comparative Analysis of Lithium-Ion Battery Resistance Estimation Techniques for Battery Management Systems," Energies, vol. 11, 1490, 2018.

[17] L. Zheng, L. Zhang, J. Zhu, G. Wang, and J. Jiang, "Co-estimation of state-of-charge, capacity and resistance for lithium-ion batteries based on a high-fidelity electrochemical model," Applied Energy, vol. 180, pp. 424-434, 2016.

[18] G.K. Prasad, and C.D. Rahn, "Model based identification of aging parameters in lithium ion batteries," Power Sources, vol. 232, pp. 79-85, 2013.

[19] A. Lievre, A. Sari, P. Venet, A. Hijazi, M. Ouattara-Brigaudet, S. Pelissier, "Practical Online Estimation of Lithium-Ion BatteryApparent Series Resistance forMild Hybrid Vehicles," IEEE Transactions on Vehicular Technology, vol. 65, no. 6, pp. 4505-4511, 2016.

[20] S. B. Vilsen, S. K. Kær, and D.-I. Stroe, "Predicting Lithium-ion Battery Resistance Degradation using a Log-Linear Model," In Proceedings of 2019 IEEE Energy Conversion Congress and Exposition (ECCE), pp. 1136-1143, 2019.

[21] J. Meng, L. Cai, G. Luo, D.-I. Stroe, and R. Teodorescu, “Lithium-ion battery state of health estimation with short-term current pulse test and support vector machine,“ Microelectronics Reliability, vol. 88-90, pp. 1216-1220, 2018.
[22] J. Wu, Y. Wang, X. Zhang, and Z. Chen, “A novel state of health estimation method of Li-ion battery using group method of data handling,“ Power Sources, vol. 327, pp. 457-464, 2016.
[23] P. Guo, Z. Cheng, and L. Yang, “A data-driven remaining capacity estimation approach for lithium-ion batteries based on charging health feature extraction,“ Power Sources, vol. 412, pp. 442-450, 2019.
[24] D. Yang, Y. Wang, R. Pan, R. Chen, and Z. Chen, “A neural network based state-of-health estimation of lithium-ion battery in electric vehicles,“ 8th International Conference on Applied Energy, Energy Procedia, vol. 105, pp. 2059-2064, 2017.
[25] A. A. Hussein, “Adaptive Artificial Neural Network-Based Models for Instantaneous Power Estimation Enhancement in Electric Vehicles’ Li-Ion Batteries“, IEEE Transactions on Industry Applications, vol. 55, pp. 840-849, 2019.
[26] M.A. Patila, P. Tagadea, K.S. Hariharana, S.M. Kolakea, T. Song, T. Yeo, and S. Doo, “A novel multistage Support Vector Machine based approach for Li ion battery remaining useful life estimation,“ Applied Energy, vol. 159, pp. 285-297, 2015.
[27] V.T. Trana, H.T. Phama, B.-S. Yanga, and T.T. Nguyen, “Machine performance degradation assessment and remaining useful life prediction using proportional hazard model and support vector machine,“ Mechanical Systems and Signal Processing, vol. 32, pp. 320-330, 2012.
[28] P. Olofsson and M. Andersson, “Probability, statistics, and stochastic processes,” 2nd edition, Wiley 2012.
[29] D.-I. Stroe, ”Lifetime Models for Lithium-ion Batteries used in Virtual Power Plant Applications,” PhD Thesis, Aalborg University, 2014.
[30] A. Gismero, E. Schaltz, and D.-I. Stroe, ”Recursive State of Charge and State of Health Estimation Method for Lithium-Ion Batteries Based on Coulomb Counting and Open Circuit Voltage,” Energies 2020, vol. 13, pp. 1-11, 2020.